

---

This is an electronic reprint of the original article.  
This reprint may differ from the original in pagination and typographic detail.

Mirmoosa, M.S.; Ruting, F.; Nefedov, I.S.; Simovski, C.R.

**Effective-medium model of wire metamaterials in the problems of radiative heat transfer**

*Published in:*  
Journal of Applied Physics

*DOI:*  
[10.1063/1.4883239](https://doi.org/10.1063/1.4883239)

Published: 01/01/2014

*Document Version*  
Publisher's PDF, also known as Version of record

*Please cite the original version:*  
Mirmoosa, M. S., Ruting, F., Nefedov, I. S., & Simovski, C. R. (2014). Effective-medium model of wire metamaterials in the problems of radiative heat transfer. *Journal of Applied Physics*, 115(23), Article 234905. <https://doi.org/10.1063/1.4883239>

---

This material is protected by copyright and other intellectual property rights, and duplication or sale of all or part of any of the repository collections is not permitted, except that material may be duplicated by you for your research use or educational purposes in electronic or print form. You must obtain permission for any other use. Electronic or print copies may not be offered, whether for sale or otherwise to anyone who is not an authorised user.

## Effective-medium model of wire metamaterials in the problems of radiative heat transfer

M. S. Mirmoosa, F. Rütting, I. S. Nefedov, and C. R. Simovski

Citation: [Journal of Applied Physics](#) **115**, 234905 (2014); doi: 10.1063/1.4883239

View online: <https://doi.org/10.1063/1.4883239>

View Table of Contents: <http://aip.scitation.org/toc/jap/115/23>

Published by the [American Institute of Physics](#)

---

### Articles you may be interested in

[Layered thermal metamaterials for the directing and harvesting of conductive heat](#)

[AIP Advances](#) **5**, 053403 (2015); 10.1063/1.4916220

[Super-Planckian near-field thermal emission with phonon-polaritonic hyperbolic metamaterials](#)

[Applied Physics Letters](#) **102**, 131106 (2013); 10.1063/1.4800233

[Broadband super-Planckian thermal emission from hyperbolic metamaterials](#)

[Applied Physics Letters](#) **101**, 131106 (2012); 10.1063/1.4754616

[Tunable quasi-monochromatic near-field radiative heat transfer in s and p polarizations by a hyperbolic metamaterial layer](#)

[Journal of Applied Physics](#) **121**, 013106 (2017); 10.1063/1.4973530

[Near-field radiative thermal transport: From theory to experiment](#)

[AIP Advances](#) **5**, 053503 (2015); 10.1063/1.4919048

[Near-field thermal radiation between hyperbolic metamaterials: Graphite and carbon nanotubes](#)

[Applied Physics Letters](#) **103**, 213102 (2013); 10.1063/1.4832057

---

**AIP** | Journal of Applied Physics SPECIAL TOPICS



## Effective-medium model of wire metamaterials in the problems of radiative heat transfer

M. S. Mirmoosa,<sup>1,a)</sup> F. Rütting,<sup>2,b)</sup> I. S. Nefedov,<sup>1,c)</sup> and C. R. Simovski<sup>1,d)</sup>

<sup>1</sup>*Department of Radio Science and Engineering, School of Electrical Engineering, Aalto University, P. O. Box 13000, 00076 Aalto, Finland*

<sup>2</sup>*Departamento de Física Teórica de la Materia Condensada and Condensed Matter Physics Center (IFIMAC), Universidad Autónoma de Madrid, E-28049, Spain*

(Received 14 March 2014; accepted 2 June 2014; published online 17 June 2014)

In the present work, we check the applicability of the effective medium model (EMM) to the problems of radiative heat transfer (RHT) through so-called wire metamaterials (WMMs)—composites comprising parallel arrays of metal nanowires. It is explained why this problem is so important for the development of prospective thermophotovoltaic (TPV) systems. Previous studies of the applicability of EMM for WMMs were targeted by the imaging applications of WMMs. The analogous study referring to the transfer of radiative heat is a separate problem that deserves extended investigations. We show that WMMs with practically realizable design parameters transmit the radiative heat as effectively homogeneous media. Existing EMM is an adequate tool for qualitative prediction of the magnitude of transferred radiative heat and of its effective frequency band. © 2014 AIP Publishing LLC. [<http://dx.doi.org/10.1063/1.4883239>]

### I. INTRODUCTION

Metamaterials are effectively homogeneous composite media possessing unusual properties, which are not observed for natural materials. Electromagnetic metamaterials are composites realizing unusual and useful functionalities with electromagnetic radiation. One of the most interesting classes of electromagnetic metamaterials are so-called hyperbolic metamaterials (see, e.g., Refs. 1–5). They display hyperbolic (also called indefinite) dispersion, i.e., their isofrequency surfaces in the reciprocal space have a hyperbolic shape. This dispersion results from the different signs of the principal components of the effective permittivity or/and permeability tensor. In dielectric hyperbolic metamaterials, the tensor of the effective permittivity has one negative and two positive components, or one positive and two negative components. More exactly, this sign refers to the real parts of these components, whereas imaginary parts are assumed to be sufficiently small. In this paper, we do not consider magnetic hyperbolic metamaterials (that the principal components of their effective permeability tensor possess different signs). They are not so interesting for us, since all known examples of such composites have the hyperbolic dispersion in a rather narrow frequency range. We are interested in broadband hyperbolic metamaterials, and hence, we will concentrate in the following on dielectric hyperbolic metamaterials.

The electromagnetic fields created by internal or boundary sources in a dielectric hyperbolic metamaterial possess many interesting features such as strong enhancement of radiation, extraordinary directionality, amazing spatial distribution of radiation, and others (see, e.g., the overview in Ref. 5). These effects originate from the general property of

hyperbolic metamaterials—an extremely broad spatial spectrum of propagating waves. The maximal wave number of propagating waves in these metamaterials is restricted only by the internal granularity of the composite and is much larger than the wave number in free space  $k_0 = \omega/c$ . Hyperbolic dispersion in effectively dielectric media had been known earlier—this is the property of cold magnetized plasma. However, eigenwaves in magneto-plasma are different from those in hyperbolic metamaterial due to the non-reciprocity of this plasma. Its permittivity tensor comprises non-zero off-diagonal components that attracted the main attention of researchers. Such implications of hyperbolic dispersion for internal sources as the enhancement of their radiation compared to that in free space (so-called Purcell's factor) and the conical radiation pattern had been known earlier.<sup>6</sup> Other implications have been only studied starting from the paper by Smith and Schurig,<sup>1</sup> which attracted a lot of attention to solid hyperbolic metamaterials. Among these implications, it worth to mention the extremely high intensity of radiative heat in the near vicinity of a hot hyperbolic metamaterial.<sup>7–9</sup> Another exciting effect was considered in Ref. 10 where it was suggested to use wire metamaterials (WMMs) to achieve giant enhancement of the radiative heat transfer (RHT) through the micron-thick gap between two bodies. Later a number of works dedicated to the use of hyperbolic metamaterials for molding the thermal radiation have been published, e.g., Refs. 7–9, 11–16. This rapidly grown literature has responded to the modern challenge—the necessity to enhance heat-harvesting systems. The heat harvesting and its conversion into electricity is one of the most important challenges for the modern world. Hyperbolic metamaterials are definitely promising for these applications, especially for thermophotovoltaic (TPV) systems. Investigations of TPV systems enhanced by metamaterials are becoming now a new branch of the modern literature. Though this recently awakened interest is mainly

<sup>a)</sup>Electronic mail: mohammad.mirmoosa@aalto.fi

<sup>b)</sup>Electronic mail: felix.rutting@uam.es

<sup>c)</sup>Electronic mail: igor.nefedov@aalto.fi

<sup>d)</sup>Electronic mail: konstantin.simovski@aalto.fi

triggered by applications, the lack of basic knowledge about radiative heat fluxes in metamaterials requires of researchers to concentrate, first, on fundamental issues. Among these issues, there is the problem of the adequate homogenization of metamaterials in the context of RHT. An important type of these metamaterials is WMM, a class of hyperbolic metamaterials, for which the homogenization theory has been developed quite well. Then, our problem can be formulated as the investigation of the applicability of existing effective medium model (EMM) to WMMs for the adequate description of RHT. The bounds of validity of the EMM for WMMs have been already outlined for all practically important variants of WMMs operating in many ranges from microwaves to visible light. However, this question needs to be revisited because the previous studies were targeted to the imaging applications of WMMs. The adequacy or inadequacy of the EMM for this application can not be transferred directly to the adaptability of EMM for RHT purposes (e.g., for TPV systems). This paper is the study of the applicability of EMM for RHT over the micron-scale path through WMMs of metal nanowires operating in the near infrared (IR) range (1.5–6  $\mu\text{m}$  or 50–200 THz). Here, we investigate several geometries that may correspond to so-called micro-gap TPV systems. These geometries seem to be promising in view of our previous researches related to these systems. TPV systems, and especially micro-gap ones, do not represent a common knowledge for the broad scope of physicists and opticians. Therefore, the next section starts with brief overview of TPV systems, and it outlines how WMMs can be used for increasing their efficiency. After this introduction, it becomes clear which structures based on WMMs are relevant in order to test the applicability of EMM. We also explain the difference between the application of EMM to RHT and to imaging problems. We hope that this overview section will be instructive for an amount of readers.

## II. PROSPECTIVES OF MICRO-GAP TPV SYSTEMS AND WIRE METAMATERIALS FOR THEIR ENHANCEMENT

All TPV systems (see, e.g., in Refs. 17 and 18) are based on the photovoltaic (PV) effect like solar cells. However, they operate in the IR range and comprise a hot emitter usually performed as a layer of lossy medium whose electromagnetic properties in the operational band mimic those of a black body. On its front side, the emitter is as a rule connected with the heat source in order to have a temperature as close as possible to the one of the source. At the rear side of the emitter, a PV cell is located whereas the layer of PV semiconductor is separated from the emitter by a gap. In far-field TPV systems, the gap is an optically very large air gap. In some TPV systems, the gap is very thin (below 1 mm) and it is filled with a low-pressure inert gas in these cases. Some other TPV systems have even a sub-micron gap between the emitter and the PV medium. Then, the TPV system is insulated from the atmosphere, and the emitter is separated from the PV cell by a vacuum gap.

This separation is needed in order to prevent the convection of heat across the system. This convection would

excite high-temperature phonons in the semiconductor, suppressing the PV effect.<sup>19</sup> The heating of the PV medium by the thermal radiation of the emitter also results in the excitation of phonons. It is a harmful effect restricting the overall efficiency of the PV conversion. It is clear that a part of the frequency spectrum of the thermal radiation is below the semiconductor bandgap, and therefore, it is fully harmful. This radiation is fully dissipated. To avoid this unwanted effect, PV cells are often furnished with a multilayer dielectric stack, which reflects low-frequency radiation and decreases the reflection of useful high-frequency one.

However, high-frequency radiation is converted into photocurrent only partially, and the radiative heating cannot be fully avoided. Therefore, TPV systems are furnished by a convective heat sink located at the rear side of the PV cell. Depending on the practical design, the last one can be a cold water pipe, an air ventilation, or a massive metal plate. Sometimes even cryogenic cooling systems are involved.

Small TPV systems may serve as temperature sensors. Large-area TPV systems operating in the near IR band may harvest and convert heat from specially designed combustors or from the flue gases of industrial furnaces. In these systems, the emitter produces a significant radiative heat flux and the power output per unit area of the emitter can attain several  $\text{W}/\text{cm}^2$ .<sup>18</sup>

Solar TPV systems, first suggested in Ref. 20, are very exciting power generators, which have been rapidly developed throughout the past decade.<sup>18,21–23</sup> In these systems, the energy of solar light is harvested by focusing mirrors or lenses and concentrated into a narrow light beam illuminating an optical absorber. This absorber serves as an intermediate heat source for a frequency-selective emitter. Joining an absorber and an emitter into one metamaterial structure, one achieves maximal possible heating.<sup>24</sup> Fitting the band of resonant emission to the photovoltaic band and exploiting the geometric factors<sup>21</sup> one may achieve a surprisingly high (45%) efficiency for the conversion of incident solar light into electricity (see, e.g., Refs. 21–23). However, the first known experimental sample with flat metamaterial emitter has shown only 3.2% efficiency.<sup>25</sup>

In all other TPV systems, the emitter is in mechanical contact with the heat source and usually acquires its temperature. Then, the radiative heat flux between the hot (emitter) and cold media separated by an optically thick gap  $d > \lambda_{\text{max}}$  cannot exceed that between two black bodies on the same temperatures  $T_1 > T_2$ . Here,  $\lambda_{\text{max}}$  is the maximal wavelength of the effective radiation band, and  $T_1$  refers to the emitting medium and  $T_2$  to the PV medium and/or to the media of anti-reflecting filter covering it. In the best case, RHT corresponds to the Planckian limit and can be written as

$$B_\omega = B_{1\omega} - B_{2\omega} = \frac{k_0^2}{4\pi^3} (\Theta(T_1) - \Theta(T_2)),$$

$$\Theta(T) = \frac{\hbar\omega}{\left(\frac{\hbar\omega}{e^{k_B T}} - 1\right)}. \quad (1)$$

Here,  $B_{1,2\omega}$  is the frequency spectrum of power radiated from a unit surface of semi-infinite black body 1 or 2 in free

space,  $\hbar$  and  $k_B$  are Planck's and Boltzmann's constants, respectively. Strictly speaking, formula (1) is an approximation—is not fully exact even for black bodies. Really, the non-zero thermal flux directed from the hot medium to the cold one due to the temperature gradient contradicts to the condition of the thermal equilibrium on which the Planckian theory of thermal radiation was built. However, when the energy heat transfer per unit area is small compared to the heat stored under the unit surface of the emitting black body the approximation (1) is adequate. This is the case of far-field TPV systems—the applicability of (1) for them is not disputable since is confirmed by long practice.

In the so-called near-field TPV systems when the gap  $d$  between the emitting and the PV media is strongly sub-micron the RHT turns out to be super-Planckian, i.e., exceeds the RHT between black bodies, as given in Eq. (1). Super-Planckian RHT was first predicted by Rytov in his pioneering book<sup>26</sup> where he studied the heat transferred from a lossy dielectric half-space to a perfect metal through a vacuum gap  $d$  much narrower than the minimal wavelength of emission  $\lambda_{\min}$ . The approach by Rytov was later developed in the seminal work by Polder and Van Hove<sup>27</sup> who obtained an elegant closed-form solution for two lossy half-spaces separated by an optically narrow gap. The reason of the super-Planckian RHT for  $d \ll \lambda_{\min}$  is the photon tunneling effect. This effect revealed by Newton (and explained using the wave theory of light by Fresnel) is the power transfer by a pair of mutually coherent evanescent waves (incident one and reflected one). The effect occurs when two media separated by the gap  $d$  have non-zero optical losses. Power transferred by a pair of evanescent waves depends on the complex permittivities of both media, the amplitude  $E_0$ , the spatial frequency  $q > k_0$  of the evanescent wave, and the gap thickness  $d$ . The classical studies on the implications of the photon tunneling for RHT<sup>26,27</sup> were based on the use of so-called fluctuation-dissipation theorem<sup>28</sup> introduced in 1951 by Callen and Welton. Strictly speaking, this theorem as well as the Planckian theory of thermal radiation is valid only for the thermal equilibrium. However, as it was assumed by in Ref. 26 and later re-formulated by Landauer in Ref. 29, RHT though exceeds the Planckian limit is still sufficiently weak for the validity of the equilibrium approximation.

Recent development of technologies resulted in the creation of advanced near-field TPV systems where the Newtonian photon tunneling can be enhanced for the given gap  $d$  by modification of both hot and cold surfaces. For these systems, the so-called strongly super-Planckian RHT (SSP RHT) has been predicted in a number of works (see, e.g., Refs. 30–41). We define SSP RHT as RHT exceeding the black-body limit (1) by one order of magnitude or more. A so strong RHT was predicted for the cases when the gap was as small as  $d < 100$  nm (the needed value of  $d$  depends on the frequency range in which the system operates). If the gap is as tiny as  $d = 1–10$  nm, SSP RHT holds for any practical media. When  $d = 10–100$  nm, SSP RHT is achieved involving electromagnetically coupled polaritons (either surface plasmon or surface phonon polaritons) excited at both sides of the gap. The highest RHT corresponds to the case

when the hot and the cold materials have the same complex permittivities,<sup>33</sup> or their surfaces are covered with nanolayers of the same metamaterial.<sup>34,35,42</sup>

In the case of SSP RHT, the thermal equilibrium is essentially broken, and the applicability of the corresponding approximation for calculating RHT becomes disputable. Only experiments may answer how the classical theory of RHT works for so strong thermal fluxes. The early experiments reviewed in Ref. 38 have shown the value of total RHT (integral over the frequency spectrum) across the gap  $d > 10$  nm much smaller than that predicted in Refs. 26 and 27. However, later the reason of this disagreement has been revealed. Earlier experiments were not trustful due to the high curvature of the metal probe whose tip was wrongly assumed to mimic a piece of a flat metal interface. In more recent experiments, the predictions of existing theory have been qualitatively confirmed. It was done for dielectrics separated by a nanogap in Refs. 39 and 40 and for metals in Refs. 43 and 44. The qualitative applicability of the classical theory was confirmed for  $d > 30–50$  nm. This value of  $d$  corresponds to near-field TPV systems, which were recently practically created.

The most recent experiment has shown that the classical model keeps qualitatively adequate even in the case when RHT across the nanogap is enhanced by polaritons (RHT between sheets of biased graphene<sup>45</sup>). Only for very tiny gaps  $d < 30$  nm, the experimental dependence of the magnitude of RHT on  $d$  diverges significantly from theoretical predictions. It is not surprising because the thermal equilibrium for so small gaps is violated heavily. The impact of the non-equilibrium for very high thermal fluxes was studied in Ref. 46 where some corrections to the classical model of RHT have been introduced. Also, the quantum friction and Casimir forces may modify the classical model for so small gaps.<sup>31</sup> So, the classical model of RHT in near-field TPV systems, based on the equilibrium approximation, though not very accurate allows rather adequate predictions—the order of magnitude for SSP RHT and the frequency band in which SSP RHT holds are predicted correctly.

In spite of the dramatic gain compared to the black-body limit, near-field TPV systems are usually considered as not promising for such applications as cooling of objects and generation of electricity. Though in Ref. 41 the non-zero perspectives of these systems as electric generators were claimed, in the literature one can find pessimistic objections (see, e.g., Refs. 18 and 47). First, the parallelism of two slabs with nanometer vacuum gap between them is practically realizable only over a very small area. Second, maintaining this parallelism with sub-nanometer quality makes a near-field TPV system quite expensive not only in what concerns its fabrication but also in its exploitation. Third, these systems have an intrinsic electromagnetic drawback. Namely, it is difficult to avoid the heating of the PV medium by the low-frequency thermal radiation from the emitter. It is clear that the usual frequency filter cannot be combined with a nanometer gap. If the conventional optically thick dielectric stack (or a solid layer) is introduced between the PV medium and the emitter, the polariton cannot be excited at the sides of the nanogap, and the main mechanism of SSP RHT

exploited in near-field TPV systems is not realized. Therefore, the nanogap in near-field TPV systems separates, namely, the PV medium from the emitter. In this situation, the low-frequency part of the thermal radiation obviously heats the PV medium and may decrease the PV generation.

Of course, this heating is avoided if the magnitude of RHT (though SSP) is small. This is possible at low temperatures. Such near-field TPV systems are not suitable for the harvesting and conversion of heat, and they can be used only as sensing and imaging devices (see, e.g., Refs. 43 and 48). Low temperatures imply the mid-IR range of radiation. Then, the cryogenic cooling of the PV cell is required because the semiconductors with narrow bandgap corresponding to the mid-IR range cannot operate at room temperatures.

The expectations of Ref. 41 on the electricity generation in near-field TPV systems were related with the frequency selectivity of the emission. Then, the frequency band of RHT may fit the operation band of the PV cell. An array of IR antennas may emit the needed narrow-band thermal radiation. However, as it was shown in Ref. 36, the presence of the PV media in the near vicinity of the nanoantenna dramatically decreases the frequency selectivity of its thermal emission. When  $d \rightarrow 0$ , the band of RHT approaches to the band of Planckian heat transfer even for a strongly resonant nanoantenna. Anyway, the recent studies allow one to revisit this issue. This prospective of frequency-selective RHT in near-field TPV systems is related with hyperbolic metamaterials (see below).

The so-called micro-gap TPV systems<sup>42,47,49–54</sup> occupy an intermediate position between conventional (far-field) TPV systems and near-field ones. The micron-thick vacuum gap allows the PV material to capture the whole radiation of the emitter and even to overcome (though rather weakly) the Planckian limit for the RHT. The emitter in these systems usually has temperatures  $T \geq 1000$  K that implies the near-IR operation band. The overall geometry of these systems is usually cylindrical; however, the radius of curvature is very large compared to the gap thickness  $d$ , and both emitting and PV surfaces can be modeled as flat ones. Since the electromagnetic absorption in these media is high, in the studies of the RHT both the emitter and PV layer can be also modeled as two half-spaces. These systems are capable to generate a noticeable electric power because they are realizable with useful surfaces of the order of one  $\text{cm}^2$  and even bigger. Special mechanical systems with spacers and springs<sup>55–57</sup> maintain the micron vacuum gap over this area with the maximal deviation 50–100 nm per  $1 \text{ cm}^2$ . The thermal conductance through the spacers (holey quartz tubes of submicron diameter) due to their sparsity does not practically worsen the PV operation. A dielectric film of submicron thickness can be introduced on top of the PV layer.<sup>47,57</sup> This film is multi-functional: it decreases the harmful mechanical tension produced by spacers, and (with properly chosen thickness) makes the electromagnetic reflection at least weakly frequency selective. However, the SSP RHT is not achievable in existing micro-gap TPV systems because the existing technology restricts the minimal thickness of the gap by  $d > 400\text{--}500$  nm. This value of  $d$  is too large for the photon tunneling through free space.

Imagine that before stacking the emitter and the PV cell to a micro-gap TPV system, we have grown two arrays of aligned metal nanowires or carbon nanotubes in both emitting medium and in the dielectric medium covering the PV cell. Let these arrays be sparse enough and let these nanowires/nanotubes contain free-standing parts. Let the averaged length of these protrusions be nearly equal  $d/2$ . Then, after stacking, we obtain free-standing linear protrusions at both sides of the gap whose ends nearly correspond to the central plane of the gap.<sup>10</sup> Such a micro-gap TPV system will have the gap completely filled with WMM. Of course, in this way, we will increase the harmful convective heat transfer. Really, to grow all identical nanowires/nanotubes is impossible. Nearly one half of them will be slightly shorter and one half—slightly longer than  $d/2$ . Some of them will intersect and touch one another. This will result in the additional (to that through the existing spacers) heat convection through the gap.

However, this effect is hopefully very small. Most of protrusions whose length exceeds  $d/2$  will not touch one another because the arrays are sparse.<sup>16</sup> One can estimate that for  $a > 2b$  (where  $a$  is the period of nanowires/nanotubes and  $b$  is their thickness) the total cross section of hot nanowires/nanotubes occasionally overlapping with cold ones turns out to be smaller than the total cross section of spacers<sup>55,57</sup> per unit area. Therefore, the increase of the convection between the emitter and the PV medium after this modification of the vacuum gap may be negligible.

Meanwhile, the radiative heat transfer will grow dramatically. The spatial harmonics of radiative heat with  $q > k_0$  (evanescent in free space) are propagating across the gap. This broadening of the spatial spectrum of the waves carrying the energy is not a resonant effect, and it happens in a wide frequency range.<sup>10</sup> This mechanism of the enhancement of RHT is very efficient and keeps even for much thicker gaps if only the nanowires could be grown so long. The micron thickness of the gap is restricted by the existing technologies which do not allow to prepare the free-standing parts of aligned nanowires longer than 500–600 nm.<sup>58</sup>

In 2011, WMM of single-wall metal-state carbon nanotubes, which can be as thin as 1–2 nm, has been considered whereas the period  $a$  can be as small as 10–20 nm.<sup>10</sup> These design parameters allow the sparsity of the array to be combined with its optical density which is the prerequisite of the EMM. The small thickness of nanotubes (which also are hollow) allowed us to neglect the absorption and generation of heat in nanotubes connected to the emitter. In the next work,<sup>16</sup> the arrays of metal nanowires have been analyzed. In order to ensure the robustness of free-standing nanowires of length 500 nm, these nanowires have to be substantially thick (at least  $b = 40\text{--}50$  nm (Ref. 58)). In order to operate as a hyperbolic metamaterial, the array should be optically dense, i.e.,  $a \ll \lambda_{\text{min}}$ . For the frequency range of thermal radiation of 50–200 THz (this range corresponds to the temperature of the emitter close to 1000 K), the last requirement practically means  $a < 200\text{--}300$  nm.

The work in Ref. 16 published in 2013 shows (using EMM) that SSP RHT is achievable for micro-gap TPV systems together with high frequency selectivity. In previously known micro-gap TPV systems<sup>42,47,50–54</sup> the heating by the

low-frequency radiation is a serious problem that restricts the PV conversion and requires a complex cooling system. Really, a micron thick gap does not allow the multilayer filter to be inserted. The frequency selectivity of the bonding dielectric film with thickness 200–300 nm (see above) is very insufficient and offers a weak frequency selectivity. However, the introduction of two arrays of nanowires into emitting and PV media (especially with different periods  $a_1 \neq a_2$  in these two media) transforms the micro-gap TPV system into an effectively multilayer structure with high optical contrast between effective-medium layers. This allows us to theoretically achieve a so high frequency selectivity that in the narrow operational band the RHT is SSP (the gain of the order 100–1000 compared to the black bodies) and beyond this band the RHT is weaker than that between two black bodies.<sup>16</sup> High frequency selectivity dramatically increases the prospectives of advanced TPV systems we have suggested, and hyperbolic metamaterials can make a breakthrough in the micro-gap TPV systems.

In 2011–2013, in works guided by Ben-Abdallah, Biehs, and Jacob,<sup>7,9,11–14</sup> similar ideas were developed for RHT through the hyperbolic metamaterials realized as a periodic stack of alternating metal and dielectric nanolayers. Here, the stress was done to the frequency selectivity of RHT when the emitter comprises a layer of hyperbolic metamaterial. The hyperbolic-medium layer supports the surface states at the interface with the vacuum gap and creates a huge density of the radiative heat stored at the surface. The presence of the closely located PV medium results in the enhanced photon tunneling because this stored energy finds the sink. This effect is frequency selective. Beyond the operational band of the PV cell the same stacked metamaterial can operate inversely—suppressing the RHT. At higher frequencies a multilayer stack becomes a 1D photonic crystal with a photonic bandgap and reflects all spatial harmonics. At low frequencies, the same hyperbolic metamaterial may not support surface states, and the photon tunneling is not enhanced.

Of course, in this design approach the vacuum gap between the hot and cold media cannot be filled with a metamaterial, and the application of this frequency-selective SSP RHT to TPV systems is possible only if the vacuum gap is optically very thin. In other words, these studies are targeted to near-field TPV systems. These results allow one to revisit the prospective of near-field TPV systems as electric generators. Moreover, the PV cell can also comprise a layer of hyperbolic metamaterial that allows further increase of the frequency selectivity. One may conclude that hyperbolic metamaterials give a new pulse to the development of near-field TPV systems.

Now let us return to micro-gap TPV systems and discuss the role of EMM in the further studies of SSP RHT through layers of WMMs. The work in Ref. 16 claims the giant potential of WMMs for improvement of the micro-gap TPV systems. However, all results were obtained within the framework of EMM. The applicability of this EMM to such problems was partially validated only for single-wall metal-state carbon nanotubes.<sup>10</sup> Huge potential of WMMs of metal nanowires for frequency-selective SSP RHT needs to be

confirmed by full-wave simulations. These simulations can be performed as follows.

Following the classical approach, the mean value of the radiative heat in the 1D problem is expanded into double Fourier integral over frequencies  $\omega$  and spatial frequencies  $q$ . Here, spatial frequency is defined as the transverse component of the wave vector of a spatial harmonic. This value is scalar because the problem is isotropic in the horizontal plane. Assume for simplicity of calculations, that the WMM is a strictly periodic array. Since spatial harmonics transfer the heat independently, one can simulate the power transmittance of every spatial harmonic at every frequency reducing the boundary problem of the array to the cell problem. This approach allows the utilization of existing simulation software. Next, the frequency spectrum of thermal power transmittance can be obtained by integration of the harmonic power transmittance over  $q$ . Such the study is cumbersome and time-consuming; however, it is fully realistic in order to check the applicability of EMM for RHT in micro-gap TPV systems.

A natural question arises: why do we need to use an approximate EMM, if the full-wave simulations can be done for predicting the RHT? There are two reasons for it. First, the search of the optimal parameters through numeric simulations will be very long. Second, commercial software only allow us to calculate the heat transferred from the solid emitter to the solid PV medium. They do not allow calculations of radiative heat in nanowires. In Ref. 10, we performed exact calculations using the home-made code only because we could neglect the heat absorbed in and produced by carbon nanotubes. This negligence makes sense because nanotubes are extremely thin and hollow. In the case of metal nanowires we cannot neglect this microscopic heat. The radiative heat is absorbed and produced by every nanowire partially hosted in the medium and partially free-standing in the gap. These nanowires electromagnetically interact with other nanowires. This microscopic problem is extremely difficult for the exact solution; moreover, that one has to match the microscopic radiative heat to the total macroscopic RHT.

In Ref. 16, the EMM has been used, assuming that the layers of WMMs have a step-wise (uniform across every layer) temperature distribution. These temperatures are in between the temperature of the emitter and that of the PV medium. Even in this simple formulation, the problem of radiative heat exchange between piece-wise isothermal effective media is much more difficult than the heat exchange through the vacuum gap. To solve the problem of RHT in the multilayer stack, one needs a special computational apparatus. This apparatus may be the method of Green's function for step-wise temperature distribution in a layered structure. This method was successfully applied for metal-dielectric stacks in Refs. 11–14. However, for layers of WMMs, this method would require a difficult generalization because WMM is an essentially anisotropic material. Moreover, WMM is a spatially dispersive material. If the spatial dispersion effects are noticeable, the Green function method is hardly helpful. The work in Ref. 59 has suggested another method called the circuit model of RHT. This computational approach is targeted to the radiative heat produced

and absorbed in flat multilayers filled with arbitrary media—anisotropic, lossy, and spatially dispersive. This method was applied in Ref. 16 for the step-wise temperature distribution across the stack of effective media, i.e., it was combined with EMM. However, it has been unclear that if EMM is applicable for such stacks.

Notice, that even for layered hyperbolic metamaterials the applicability of the EMM is an actual problem since the strict approach based on the Green function is not free of computation errors. The error accumulates in the solution when the number of nanolayers grows. Even for the layered implementation of hyperbolic metamaterials, EMM is an important computation tool because the homogenization allows a dramatic reduction of the amount of involved layers. In recent work,<sup>60</sup> a detailed study of the bounds of validity of EMM for these metamaterials has been done. The general conclusion is rather negative. The surface plasmon polaritons excited by radiative heat at the metal-dielectric interfaces drastically limit the applicability of EMM for radiative heat transferred by the TM-polarized waves. For the TE-polarization the EMM turns out to be adequate. However, for these waves, the hyperbolic metamaterials do not promise a strong impact.

The applicability of the EMM for both types of hyperbolic metamaterials—WMMs and layered hyperbolic media was analyzed in the past decade. Several papers refer to the hyperbolic metamaterials operating in the IR range (see, e.g., Refs. 61–66). However, as it was already mentioned, all these works were targeted to the transport of near-field images across metamaterial layers. It was shown that EMM is a rather adequate tool for the prediction of the complex transmission in layers of WMMs except the case of thick wires  $2b > a$  and the case of very optically thin layers of WMM. However, the error over both frequency axis  $\omega$  and axis of spatial frequencies  $q$  is non-zero and this error grows along both these axes. What is the integral impact of this error?

From one point of view, the problem of RHT seems to be less demanding than the problem of the image transport where the transmission phase is important. Here, only the power transmittance needs to be predicted properly. Moreover, the power transmittances for individual spatial harmonics are not very relevant. Only the integral over the spatial spectrum  $q$  is important. However, this integral effect can be more demanding to the accuracy if the errors for spatial harmonics are accumulated in the integration. Also, the role of spatial harmonics with highest values of  $q$ , e.g.,  $\pi/2a < q < \pi/a$ , can be important. In the imaging problem, only spatial harmonics  $q < \pi/2a$  are important because the spatial resolution is restricted by the limit  $2a$ , smaller details cannot be resolved. Therefore, the bounds of validity of EMM for the problems of RHT and for the imaging problems may be different.

In the next section, we analyze the applicability of EMM to the structure corresponding to a prospective micro-gap TPV system with metal nanowires grown on one side of the micron gap—in the emitter. The cold part is modeled as a solid half-space covered by a solid nanolayer (the bonding film that may also increase the frequency selectivity). A nanogap between the ends of nanowires and the nanolayer is left. In this design solution, hot nanowires will not

practically touch the bonding film if the nanogap exceeds the statistic deviation of their length. Alternatively, one can locate nanowires on the cold side. In the case under study, the hot and cold media have the same permittivities, and the results for RHT will not change after such a replacement.

### III. NANOWIRES ON ONE SIDE OF THE GAP

#### A. Effective-medium models of wire metamaterials

In the overview paper, Ref. 67, two known EMMs of WMMs (the quasi-static one and the non-local one) are reviewed. Both of them describe the optical properties of these media through a uniaxial dyad of effective permittivity

$$\bar{\epsilon} = \epsilon^{\parallel} \mathbf{u}_z \mathbf{u}_z + \epsilon^{\perp} (\mathbf{u}_x \mathbf{u}_x + \mathbf{u}_y \mathbf{u}_y), \quad (2)$$

where  $\epsilon^{\parallel}$  is the axial component of the dyadic tensor and  $\epsilon^{\perp}$  is the transverse component.

The quasi-static homogenization formulas are often used to calculate these two scalar parameters for WMMs of nanowires operating at optical frequencies (see, e.g., Ref. 67)

$$\begin{aligned} \epsilon^{\perp} &= \epsilon_h \frac{\epsilon_m(1+f) + \epsilon_h(1-f)}{\epsilon_m(1-f) + \epsilon_h(1+f)}, \\ \epsilon^{\parallel} &= f\epsilon_m + (1-f)\epsilon_h, \end{aligned} \quad (3)$$

where  $\epsilon_h$  and  $\epsilon_m$  are the complex permittivities of a host medium and a metal, respectively, and  $f = \pi r_0^2/a^2$  is the metal fraction ( $b = 2r_0$  is the wire thickness and  $a$  is the array period). This simple model expresses a static mixing rule for optically dense arrays of parallel cylinders. This mixing rule describes a WMM in the IR range as a hyperbolic medium if the metal fraction is not very small. Since in the IR range for the majority of metals  $\text{Re}(\epsilon_m) \leq -60$  and  $\text{Re}(\epsilon_h) \leq 15$  for all known dielectrics and semiconductors, the negative axial permittivity  $\text{Re}(\epsilon^{\parallel}) < 0$  is ensured if  $f > 0.2$ . WMM of gold or tungsten nanowires is hyperbolic in the range of 50–200 THz if  $f > 0.19$  ( $a = 2b$ ) for host media of permittivity  $\epsilon_h = 15$ . In Refs. 61–63, a more accurate model has been developed. This model was claimed applicable from microwaves to the visible light in the condition  $r_0 \ll a \ll \lambda_{\text{min}}$ . The corresponding effective permittivity in the range of radio frequencies where metals have a very high conductivity (i.e.,  $\epsilon_m \rightarrow i\infty$ ) transits to the classical Drude-like model treating the WMM as an effective plasma.<sup>68</sup> This transition is not possible for the simplistic model (3). Notice that in the classical model by Brown,<sup>68</sup> only the propagation of waves in the plane orthogonal to wires has been studied, and the spatial dispersion effects were analyzed much later. The advanced EMM is spatially dispersive. It implies the non-local (depending on the axial wave number) effective permittivity whose components are expressed as follows:

$$\begin{aligned} \epsilon^{\perp} &= \epsilon_h + \frac{2\epsilon_h}{\frac{\epsilon_m + \epsilon_h}{f(\epsilon_m - \epsilon_h)} - 1}, \\ \epsilon^{\parallel} &= \epsilon_h + \frac{\epsilon_h}{\frac{\epsilon_h}{f(\epsilon_m - \epsilon_h)} - \frac{k_h^2 - \beta^2}{k_p^2}}. \end{aligned} \quad (4)$$

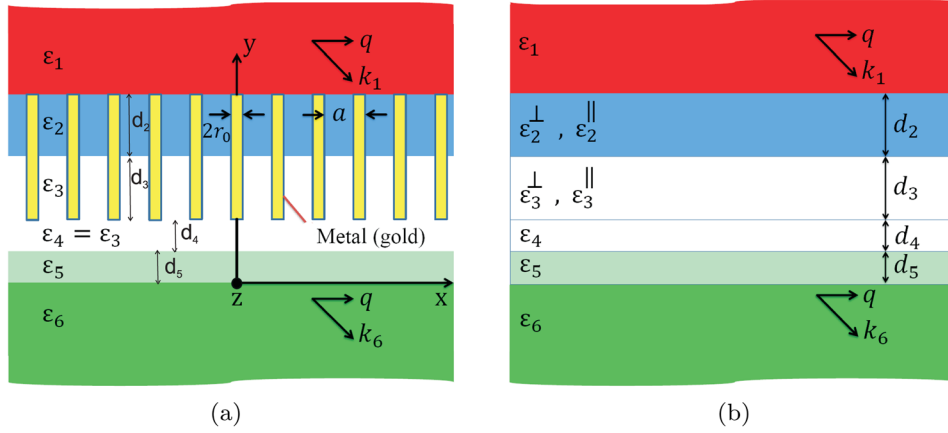


FIG. 1. (a) Schematic view of the original 6-layer structure. (b) Its effective-medium (step-wise homogeneous) model.

Here,  $k_h = k_0\sqrt{\epsilon_h}$  is the host-medium wave number,  $k_p = \sqrt{2\pi/(\ln(a/2\pi r_0) + 0.5275)}/a$  is the wave number of the effective plasma, and  $\beta$  represents the axial component of the effective medium wave number. In the near IR range, by evaluating these equations for the gold with  $\text{Re}(\epsilon_m) < -\epsilon_h$ , the real part of  $\epsilon^\perp$  is usually positive and the real part of  $\epsilon^\parallel$  is negative. This is the feature of a hyperbolic metamaterial. More details on hyperbolic dispersion in WMMs can be found in Ref. 67.

The substitution of (4) into Maxwell's equations with fixed spatial frequency  $q$  gives three solutions for  $\beta$ . For the TE-polarized (ordinary) waves, we have one solution  $\beta = \sqrt{k_0^2\epsilon^\perp - q^2}$ . In this paper, we concentrate on the RHT carried by TM-waves because WMM practically does not affect the radiative heat transferred by TE-waves. For the TM-polarization, there are two other solutions. When the parameter  $k_c$  defined as  $k_c^2 = -\epsilon_h k_p^2 / f(\epsilon_m - \epsilon_h)$  has the absolute value smaller than  $k_p$ , one of them corresponds to a quasi-TEM wave  $\beta \approx k_0\sqrt{\epsilon^\perp}$ , independent on  $q$ . In the lossless WMM this wave would be strictly TEM. Then, the second solution is an evanescent (pure imaginary  $\beta$  in the lossless limit  $\text{Im}(\epsilon_m) = 0$ ) wave. When  $|k_c| > k_p$ , both TM-solutions are propagating waves (have pure real  $\beta$  in the lossless limit). In both these situations, the advanced EMM takes both solutions into account since besides the non-local permittivity tensor this model also comprises additional boundary conditions.<sup>64</sup>

Substituting  $\beta = k_0\sqrt{\epsilon^\perp}$  into (4) yields these formulas to the form (3). To assume that the evanescent eigenwave in the layer of WMM is excited weakly and the main wave is quasi-TEM, is the same as to adopt the quasi-static mixing rule. In other words, the simplified variant of EMM is equivalent to the quasi-TEM approximation of the advanced EMM. This approximation is justified in the imaging problems for sufficiently thick layers of WMM.<sup>61-64</sup> However, it can be not justified for RHT even for optically substantial layers of WMM. This needs to be checked.

## B. Structure under study

The first structure under study is depicted in Fig. 1(a). The square array of aligned gold nanowires with period  $a \ll \lambda_{\min}$  is assumed to be grown in the host medium of

permittivity  $\epsilon_2$  so that nanowires have free-standing parts of length  $d_3$ . Between the ends of nanowires and the layer 5 ( $\epsilon_5$ ) (covering the medium 6 ( $\epsilon_6$ ), which models the PV medium of the TPV system), there is a vacuum gap  $d_4$ . This design solution can be applied to prospective micro-gap TPV systems. Then, there is no need to prepare the nanowires in the bonding film (layer 5) covering the PV medium. Free-standing nanowires are fabricated only in the emitter. Their averaged length is taken smaller than the vacuum gap thickness  $h = d_3 + d_4$  so that the practical deviations of this length ( $\pm d_4$ ) do not allow hot nanowires to touch the bonding film. Medium 1 is assumed to be an isotropic semiconductor ( $\epsilon_1 \gg 1$ ), and the radiative heat is transferred to its boundary (interface  $y = d_2 + d_3 + d_4 + d_5$ ) by propagating waves, which may have in this highly refractive medium the high spatial frequency  $q \gg k_0$ . This spatial frequency is related to the internal incidence angle  $\theta$  as  $q = k_0\sqrt{\epsilon_1} \sin \theta$ , i.e.,  $q_{\max} = k_0\sqrt{\epsilon_1}$  is the upper bound of spatial frequencies responsible for RHT.

Nanowires in host medium  $\epsilon_2$  and in free space  $\epsilon_3 = 1$  form two effectively homogeneous layers of WMMs. The vacuum gap (layer 4) in which spatial harmonics  $k_0 < q < q_{\max}$  are evanescent is assumed to be very tiny (its thickness is determined by fabrication tolerances of nanowires). Therefore, we may expect strong photon tunneling through it. The same structure described by EMM is shown in Fig. 1(b).

Since the goal of the present study is to validate the EMM and not to optimize the prospective TPV system, the parameters of the original structure were chosen arbitrary. Only the period and the radius of gold nanowires were chosen so that the TM-roots of the dispersion equation of WMMs correspond to the propagating waves. The set of parameters is presented in Table I.

Of course, the heat cannot be generated in medium 1 having purely real permittivity  $\epsilon_1$ ; however, there is no contradiction. To have in mind the emitting half-space one should obviously assume non-zero losses in medium 1. A

TABLE I. The first structure under study: host media permittivities and dimensions.

$\epsilon_1$	$\epsilon_2$	$\epsilon_3$	$\epsilon_4$	$\epsilon_5$	$\epsilon_6$	$d_2$	$d_3$	$d_4$	$d_5$	$a$	$r_0$
10	15	1	1	15	10	500 nm	300 nm	10 nm	10 nm	100 nm	25 nm

small imaginary part ( $\text{Im}(\varepsilon_1) < 0.1$ ) added to  $\varepsilon_1 = 10$  did not practically change our results. Alternatively, one can also assume that medium 1 is lossless but has finite thickness and the heat is generated on top of it. Similar speculations can be referred to medium 6—either we have in mind a small imaginary part of  $\varepsilon_6 = 10$  or our RHT refers to the thermal radiation from the bottom interface of the structure. We have calculated the axial component  $\varepsilon^{\parallel}$  of both hyperbolic media 2 ( $d_2, \varepsilon_2^{\parallel}, \varepsilon_2^{\perp}$ ) and 3 ( $d_3, \varepsilon_3^{\parallel}, \varepsilon_3^{\perp}$ ) substituting into (4) the quasi-TEM solution (that corresponds to the simplified variant of the EMM) and the TM-solution that corresponds to the evanescent wave. The results of these substitutions are presented in Fig. 2 up to 300 THz. We see that the values of these effective permittivities are almost identical up to 200 THz. The visible difference appears only above 200 THz and only for layer 2. Therefore, it is reasonable to assume that the application of the advanced model is not justified. We will validate the simplified variant of the EMM comparing its results to those of the full-wave simulation.

### C. Transmittance of the electric field and radiative heat transfer function

RHT in the model of weak non-equilibrium (see also formula (1)) is the difference of two power fluxes: the forward one from the hot boundary to the cold one and the backward one. In the present case the hot boundary is the plane  $y = d_2 + d_3 + d_4 + d_5$  between media 1 and 2 and the cold one is the plane  $y = 0$ . Then, RHT between media 1 and 6 can be written in the form<sup>26</sup>

$$S_{16} = \left[ \int_{\omega_{1\min}}^{\omega_{1\max}} M(\omega) \Theta(\omega, T_1) d\omega - \int_{\omega_{6\min}}^{\omega_{6\max}} M(\omega) \Theta(\omega, T_6) d\omega \right], \quad (5)$$

where the values  $\omega_{1,6\min}$  and  $\omega_{1,6\max}$  are practical bounds of the thermal radiation frequency ranges corresponding to temperatures  $T_1$  and  $T_6$ , respectively. The frequency spectrum of the power transmittance through the structure (forward and backward ones are identical due to reciprocity)  $M(\omega)$  is often called RHT function. As it is clear from formula (5), RHT function  $M(\omega)$  fully describes the heat transfer between media 1 and 6, since the Plank function is just a common factor weakly depending on frequency. If the EMM adequately calculates the RHT function  $M(\omega)$ , this model can be claimed applicable. Therefore, our calculations do not

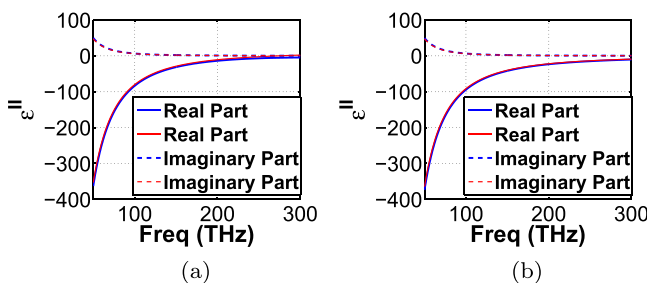


FIG. 2. The effective permittivity with substitutions of propagation factors of the TM-wave (blue color) and quasi-TEM wave (the same as the simplified EMM) (red color). (a) Layer 2 and (b) layer 3.

involve the Plank function. We compare  $M(\omega)$  calculated using EMM with that obtained by full-wave simulations.

The RHT function is related to the amplitude transmittance  $t$  of a spatial harmonic  $q$  through its spatial spectrum  $N(\omega, q)$

$$M(\omega) = \frac{1}{\pi^2} \int_0^{q_{\max}} N(\omega, q) q dq, \quad (6)$$

$$N(\omega, q) = \frac{R_1 R_6}{4|Z_6|^2} |t|^2.$$

Here,  $R_1$  and  $R_6$  are the real part of the wave impedances  $Z_1$  and  $Z_6$  of media 1 and 6, respectively.

Notice that in some works, e.g., in Ref. 10, the function  $\tau$  was used instead of  $N$ , which is equal to the Poynting vector transmittance of a spatial harmonic. The RHT can be expressed through  $\tau$  with usual coefficient  $1/4\pi^2$  corresponding to the double Fourier transform (see Ref. 10)

$$S_{16} = \frac{1}{4\pi^2} \left[ \int_{\omega_{1\min}}^{\omega_{1\max}} \int_0^{q_{\max}} \tau(\omega, q) \Theta(\omega, T_1) q d\omega dq - \int_{\omega_{6\min}}^{\omega_{6\max}} \int_0^{q_{\max}} \tau(\omega, q) \Theta(\omega, T_6) q d\omega dq \right]. \quad (7)$$

Our definition (6) follows to the work by Pendry<sup>31</sup> where it was used denoted as  $X$  to describe power transmittance of a spatial harmonic. Maximally achievable value for  $N(\omega, q)$  is equal to 0.25, whereas for  $\tau \equiv 4N$  the maximal value is, evidently, equal to unity.<sup>16,31,59</sup>

The amplitude of the transmission coefficient  $t$  for every harmonic within  $0 < q < k_0 \sqrt{\varepsilon_1}$  can be exactly calculated via full-wave simulations. For this structure, we have used the commercial software ANSYS HFSS. Alternatively, it was calculated using EMM (simplified variant) and the standard method of transfer matrices. The transfer matrix relates tangential components of electric and magnetic fields at two sides of every layer

$$F_j = \begin{pmatrix} \cos(\beta_j d_j) & -\frac{i}{Z_j} \sin(\beta_j d_j) \\ -iZ_j \sin(\beta_j d_j) & \cos(\beta_j d_j) \end{pmatrix}. \quad (8)$$

Here,  $d_j$  is the  $j$ -th layer thickness and  $Z_j$  represents its wave impedance. These impedances for TM-waves can be written as follows:

$$Z_j = \frac{\beta_j}{\omega \varepsilon_0 \varepsilon_j^{\perp}} \quad (j = 2, 3), \quad Z_j = \frac{\beta_j}{\omega \varepsilon_0 \varepsilon_j} \quad (j = 1, 4, 5, 6), \quad (9)$$

where  $\varepsilon_0$  is the free-space permittivity, and propagation factors ( $y$ -components of the wave vectors) in media 1–6 are as follows:

$$\beta_j = \sqrt{k_0^2 \varepsilon_j^{\perp} - \frac{\varepsilon_j^{\perp}}{\varepsilon_j^{\parallel}} q^2} \quad (j = 2, 3), \quad (10)$$

$$\beta_j = \sqrt{k_0^2 \varepsilon_j - q^2} \quad (j = 1, 4, 5, 6).$$

The total transfer matrix  $F_{\text{tot}}$  is obtained by multiplication of partial transfer matrices

$$F_{\text{tot}} = F_2 \times F_3 \times F_4 \times F_5 = \begin{pmatrix} F_{11} & F_{12} \\ F_{21} & F_{22} \end{pmatrix}. \quad (11)$$

Using Eq. (11), the transmission coefficient can be obtained as follows:

$$t = \frac{2}{F_{11} + Z_6 F_{12} + \frac{1}{Z_1} F_{21} + \frac{Z_6}{Z_1} F_{22}}. \quad (12)$$

The calculations using the EMM were done in a MATLAB code, which was validated by comparison with known results (for layered structures in absence of nanowires). The optical constants for gold used in both calculation models were taken from Ref. 69.

As it was already noticed, all layers of effective WMMs depicted in Fig. 1(b) are involved into RHT. Medium 4 (vacuum gap  $d_4$ ) and medium 5 (dielectric with negligible losses) do not absorb and produce the radiative heat. Thermal fluxes created by media 2, 3, and absorbed by medium 6 as well as backward fluxes created by medium 6 and absorbed in media 1–3 can be calculated using EMM.<sup>16,59</sup> In these calculations, the RHT functions corresponding to products  $F_2 \times F_3$ ,  $F_2 \times F_3 \times F_4$ , etc., would be involved. However, the RHT function  $M(\omega)$  is the most challenging for the applicability of EMM because it involves the transfer through the maximal number of intermediate layers and comprises the maximal amount of transfer matrices to be multiplied. In these multiplications, the error related with the approximation of the effective media accumulates. Therefore, we believe that it is enough to check the applicability of EMM to the radiation transfer from half-space 1 to half-space 6 through 4 intermediate nanostructured layers. If our EMM works for the transfer through 4 layers, it should work for the transfer through 1–3 layers.

#### D. Results

Fig. 3 shows the normalized flux transmittance  $N(\omega, q)$  as a function of frequency for several values of  $\theta$  ( $q = k_0 \sqrt{\epsilon_1} \sin \theta$ ). Function  $N$  is calculated using HFSS simulations and using EMM. For small angles, the agreement is very good. For large angles a frequency shift appears between the curves obtained by two methods. The oscillations of  $N(\omega)$  correspond to Fabry-Perot resonances of the whole 4-layer structure between the top and bottom interfaces. Fig. 4 shows the same double spatial-frequency spectrum of RHT as a function of  $qa$  (spatial frequency multiplied by array period) at some frequencies. The spatial frequency  $0 < q < q_{\text{max}}$  is not sufficient to show Fabry-Perot resonances.

These results correspond to a rather weak enhancement granted by nanowires compared to the black body. The RHT in the present case is not frequency selective. The reason of it is the impedance mismatch over the whole frequency range of 50–200 THz. For the given set of design parameters, all plane waves propagating in medium 1 experience strong reflections from the upper interface  $y = d_2 + d_3 + d_4 + d_5$ . Of

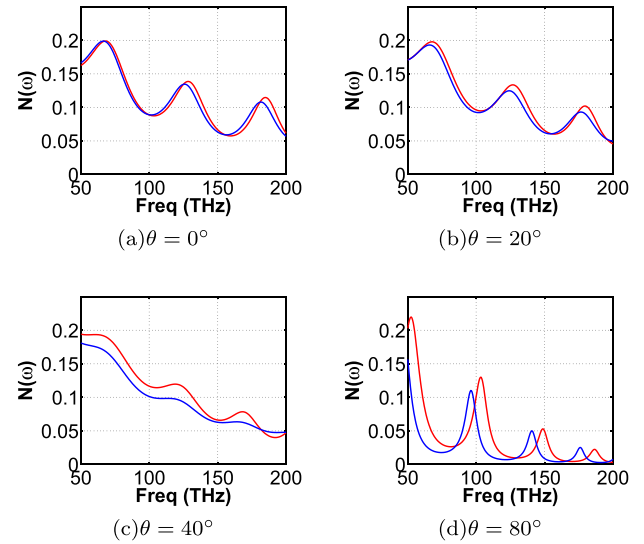


FIG. 3. Flux transmittance  $N$  versus frequency for different incidence angles. Blue and red colors correspond to EMM and simulation results, respectively. The thickness of layers 2–5 are:  $d_2 = 500$  nm,  $d_3 = 300$  nm, and  $d_4 = d_5 = 10$  nm.

course, a multilayer structure with substantial layers and high optical contrast between them is frequency selective as such. However, wave impedances of spatial harmonics depend on both  $\omega$  and  $q$ , and it is important that the good matching is achieved at some frequencies for a broad spectrum of  $q$ . This band in the present case exists but it is located at higher frequencies (where the EMM is not applicable and which are not relevant for thermal radiation with realistic temperatures). In Fig. 4, we see the mismatched regime.

Varying thicknesses of layers, it is easy to move this band into the frequency region 50–200 THz. The 2nd set of design parameters, which allows this, is presented in Table II. Notice that the vacuum gap is here multiplied by 5 compared to the previous case and the whole structure became

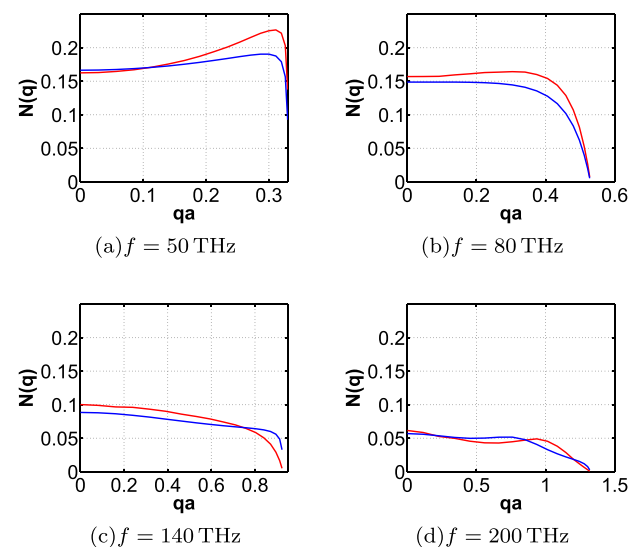


FIG. 4. Flux transmittance  $N$  versus  $qa$  for different frequencies. Blue and red colors correspond to EMM and simulation results, respectively. The thickness of layers 2–5 are:  $d_2 = 500$  nm,  $d_3 = 300$  nm, and  $d_4 = d_5 = 10$  nm.

TABLE II. The second structure under study: host media permittivities and dimensions.

$\epsilon_1$	$\epsilon_2$	$\epsilon_3$	$\epsilon_4$	$\epsilon_5$	$\epsilon_6$	$d_2$	$d_3$	$d_4$	$d_5$	$a$	$r_0$
10	15	1	1	15	10	1000 nm	750 nm	50 nm	50 nm	100 nm	25 nm

much thicker. However, within the range of 150–200 THz function  $N$  turns out to be larger than that in the previous case. Figs. 5 and 6 show the flux transmittance  $N(\omega, q)$  for the 2nd structure as a function of frequency for several values of the incidence angle and as a function of  $qa$  for several values of the frequency, respectively. The effect of better impedance matching at higher frequencies is clearly seen.

In Fig. 7, we present the heat transfer function  $M(\omega)$  calculated using the full-wave simulations and the EMM for the 1st set of the design parameters (left panel) and for the 2nd set (right panel). In both these plots, we present the same function  $M(\omega)$  calculated for the case when the nanowires are absent. Then, our Matlab code delivers an exact solution of the boundary problem. When nanowires are absent the spectrum of RHT is nearly twice as smaller as that between two black bodies separated by the same vacuum gap. This observation refers to both sets of design parameters. For the 1st set of the design parameters, nanowires grant the gain of RHT nearly equal to 2, which is therefore equal to RHT between black bodies. For the 2nd set of design parameters, the gain is frequency selective. Here, we have extended the frequency range to 250 THz ( $1.2 \mu\text{m}$ ) to illustrate better this selectivity. In accordance to EMM, the gain attains 6.5 (3.25 compared to black bodies) at 180 THz and in accordance to simulations it achieves 5.6 (2.8 compared to black bodies) at 190 THz. A further optimization that would increase the frequency selectivity of RHT offered by nanowires is possible. However, the purpose of the present paper is not the optimization but the validation of EMM. Note that the optimization

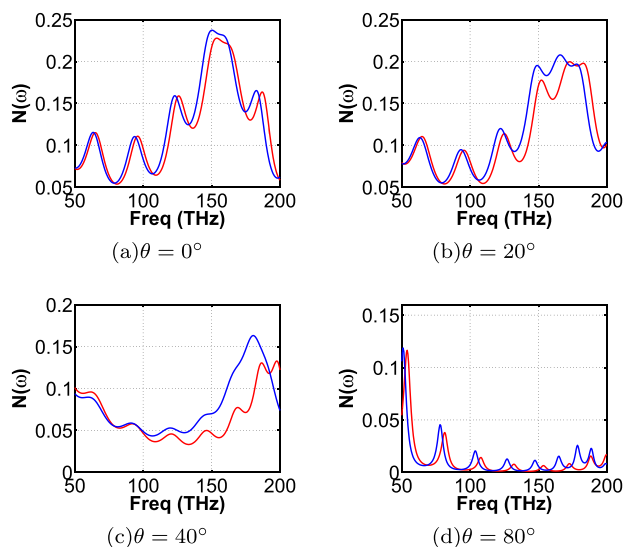


FIG. 5. Flux transmittance  $N$  versus frequency for different incidence angles. Blue and red colors correspond to EMM and simulation results, respectively. The thickness of layers 2–5 are:  $d_2 = 1000$  nm,  $d_3 = 750$  nm, and  $d_4 = d_5 = 50$  nm.

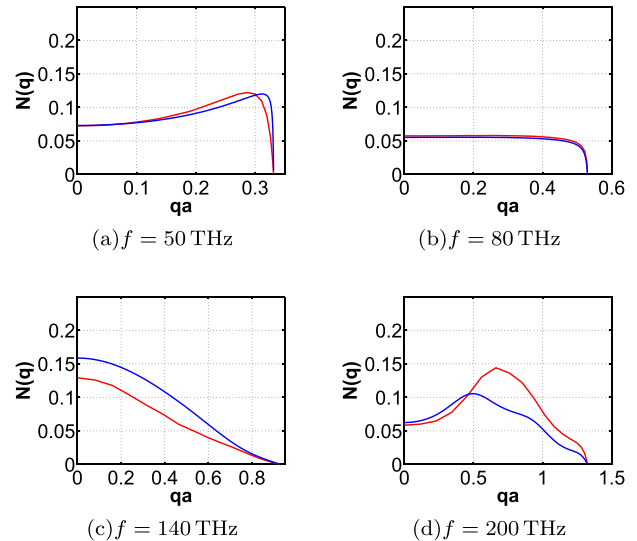


FIG. 6. Flux transmittance  $N$  versus  $qa$  for different frequencies. Blue and red colors correspond to EMM and simulation results, respectively. The thickness of layers 2–5 are:  $d_2 = 1000$  nm,  $d_3 = 750$  nm, and  $d_4 = d_5 = 50$  nm.

of the design parameters for the structure depicted in Fig. 1 does not make sense because here we consider abstract host media. The optimization of a similar structure with realistic parameters of all constitutive elements will be reported elsewhere. Here we stress on the rather good agreement between the full-wave simulations and the EMM. In the range of 50–200 THz, the disagreement in the spectrum of RHT does not exceed 25%, whereas the averaged disagreement is nearly equal 14%. It means that the agreement between EMM and simulations is very good. By using formula (5), we calculate the radiative heat flux into medium 6. We assume that the temperatures of the hot and cold media (layers 1 and 6) are 800 K and 300 K, respectively. For the first structure,  $S_{16} = 5.48 \times 10^3$  W/m<sup>2</sup> applying EMM and  $S_{16} = 6.43 \times 10^3$  W/m<sup>2</sup> according to the simulation results. As it is seen, these two values are close to each other. The situation for the second structure is even better; we have  $S_{16} = 2.76 \times 10^3$  W/m<sup>2</sup> for EMM and  $S_{16} = 2.8 \times 10^3$  W/m<sup>2</sup> based on the simulation results. Theoretical calculations of RHT in nanostructures never pretend to quantitative accuracy. They have to predict correctly the order of magnitude of the transferred radiative heat and the effective frequency band of this transfer. For the stacked implementation of hyperbolic metamaterials, simulations differ from the results

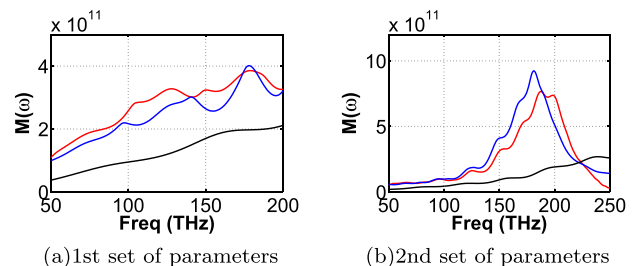


FIG. 7. Radiative heat transfer function  $M$  calculated by two methods in presence (blue and red colors corresponding to EMM and simulation results, respectively) and absence of nanowires (black color). (a) The thicknesses of layers 2–5 are:  $d_2 = 500$  nm,  $d_3 = 300$  nm, and  $d_4 = d_5 = 10$  nm. (b) The thicknesses of layers 2–5 are:  $d_2 = 1000$  nm,  $d_3 = 750$  nm, and  $d_4 = d_5 = 50$  nm.

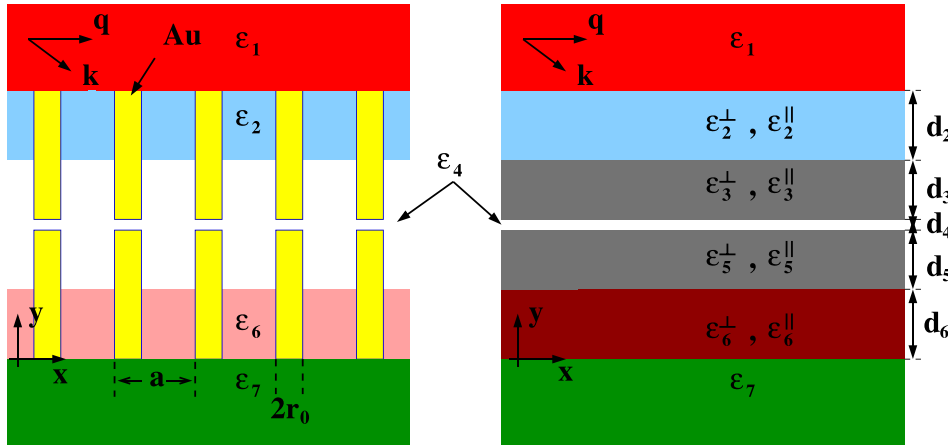


FIG. 8. Schematic view of the third structure under study, left hand figure, and its effective-medium model, right hand figure.

of EMM qualitatively.<sup>60</sup> For the present structure, the qualitative agreement between simulations and EMM has been achieved for the simplistic variant of EMM. An implementation of a more difficult non-local variant of EMM is not justified here.

#### IV. NANOWIRES ON BOTH SIDES

The similar study has been done for the design solution illustrated in Fig. 8. Now the structure of effective media comprises 7 layers (or 9 layers if we count semi-infinite layers of free space located on top and on bottom of the structure). Here two arrays of free-standing gold nanowires are hosted in dielectric layers 2 and 6 located on both sides of the gap. The heat is generated inside the top layer (medium 1) and it is absorbed in the bottom layer (medium 7). This significant modification of the previous structure (the second array of nanowires) does not worsen the agreement between full-wave simulations and EMM, although it changes the spectrum of RHT.

We have calculated the power transmittance  $N$  of spatial harmonics from the interface  $y = d_2 + d_3 + d_4 + d_5 + d_6$  to the interface  $y = 0$  through the amplitude transmittance  $t$  as above. The frequency spectrum  $M$  of RHT is obtained by the integration of  $N$  as above. Approximate calculations (EMM) were done using the apparatus of transmission (ABCD) matrices (see, e.g., Ref. 70) instead of transfer matrices  $F$  used above. Transmission matrix of a multilayer relates the amplitudes of the electromagnetic waves traveling forward and backward in the given layer with similar amplitudes in the next layer. The components of this matrix are expressed through the wave impedance  $Z$  and propagation factor  $\beta$  for an arbitrary anisotropic layer in Ref. 70. Formulas (15)–(18) of this work refer to the case of the TM-polarization on which we concentrate. Using transmission matrices, we automatically obtain the amplitude of the transmittance from layer 1 to layer 7 as a component of the corresponding matrix. The design parameters are given in Table III (parameters  $a = 100$  nm and  $r_0 = 25$  nm are the same as above).

TABLE III. The third structure under study: host media permittivities and dimensions.

$\epsilon_1$	$\epsilon_2$	$\epsilon_3$	$\epsilon_4$	$\epsilon_5$	$\epsilon_6$	$\epsilon_7$	$d_1$	$d_2$	$d_3$	$d_4$	$d_5$	$d_6$	$d_7$				
15	10	1	1	10	15	500	nm	250	nm	250	nm	10	nm	250	nm	500	nm

The software utilized for full-wave simulations was COMSOL Multiphysics, which allows in the present case better convergence than the HFSS software does. Fig. 9 shows the double spatial-frequency spectrum of RHT  $N$  as a function of  $qa$  at some frequencies. Again, in the spatial frequency  $0 < q < q_{\max}$ , no Fabry-Perot resonances can be seen. However, the frequency selectivity is here significant. As one can see in Fig. 10, the RHT is effectively concentrated within the frequency band  $f = 190$ – $230$  THz. At  $f = 210$  THz, the enhancement of transferred power spectrum granted by nanowires attains 14 in the framework of EMM and 15.5 in accordance to numeric simulations. This means that compared to the case of two black bodies, nanowires grant the frequency selective enhancement that achieves one order of magnitude in a narrow band and no enhancement outside this band. Again, this frequency selectivity is offered by the impedance matching in the effective multilayer structure.

#### V. LONG NANOWIRES

In this section, we consider the modification of the previous structure as shown in Fig. 11. Now both hot and cold

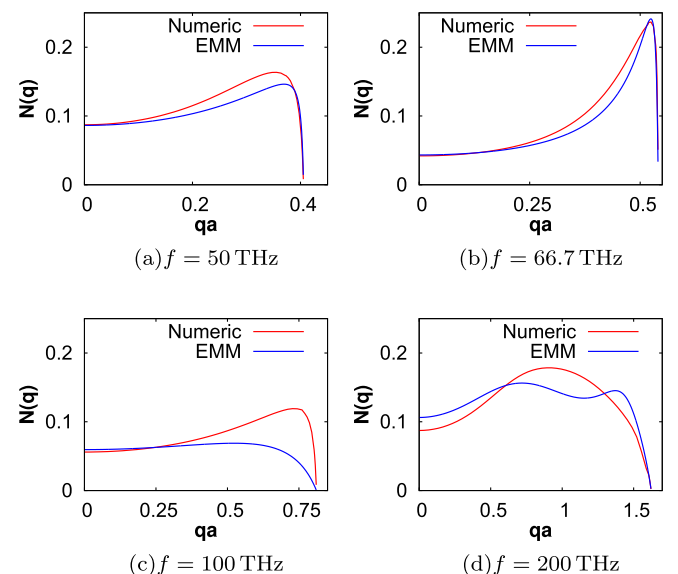


FIG. 9. Flux transmittance  $N$  versus  $qa$  (spatial frequency multiplied by area period) for different values of frequency.

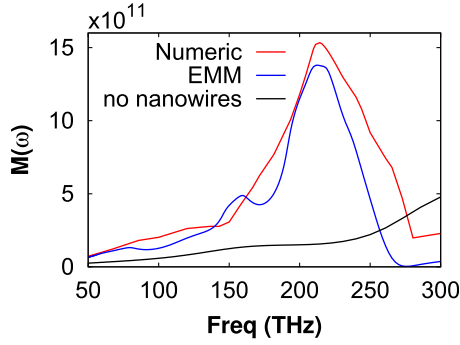


FIG. 10. Radiative heat transfer function  $M$  calculated by two methods in presence and absence of nanowires.

media are WMMs. We model them as half-spaces comprising semi-infinite nanowires. The host media are assumed to be the same—polycrystal SiC. To implement the whole hot medium as a hyperbolic metamaterial is useful if the goal is to extract more radiative heat from the depth of the emitter. Implementing also the cold medium as a hyperbolic metamaterial we achieve though imperfect but very broadband (in both frequency and spatial spectra) wave matching throughout the whole structure. This broadband matching implies the absence of frequency selectivity which is of course not a target for TPV systems. However, the goal of the present study is different. This structure is interesting by the noticeable difference between the results of local (simplified) and non-local variants of the EMM. Also, in some applications, the SSP RHT, which holds in a very broad frequency range, can be interesting because it definitely corresponds to a huge total RHT. The non-zero gap  $\delta \neq 0$  between the free-standing ends of nanowires is not relevant for the present study. Here, we assume the interdigital arrangement of cold and hot nanowires as it is shown in Fig. 11. Then, the WMM filling the gap between media 1 and 3 forms a uniform layer of medium 2.

Note, that the semi-infinite nanowires do not allow the direct use of full-wave software, which were applied in our previous sections. The spatial frequencies responsible for RHT are here restricted only by the array period  $a$ . At  $qa > \pi$ , the concept of effective medium loses validity, and our results become not trustful. However, the spatial frequency  $q$  on this bound significantly exceeds the value  $k_0\sqrt{\epsilon_1}$  which limited the RHT in our previous examples. This broad spatial spectrum would make full-wave calculations very time-consuming even if we manage to somehow define incident waves in medium 1. Therefore, in the present section, we do not validate the EMM by full-wave

simulations. We concentrate on the difference between the simplistic and the complicated models of WMM.

### A. Additional boundary conditions

Substituting (4) into Maxwell equations, one obtains the following expressions for the axial component of the wave vector:<sup>61</sup>

$$\beta^2 = \frac{1}{2\epsilon_h} \left[ \epsilon^\perp(k_h^2 - q^2) + \epsilon_h(k_h^2 + k_c^2 - k_p^2) \pm \sqrt{\left[ \epsilon^\perp(k_h^2 - q^2) - \epsilon_h(k_h^2 + k_c^2 - k_p^2) \right]^2 + 4\epsilon^\perp\epsilon_h q^2 k_p^2} \right], \quad (13)$$

where  $k_p = \sqrt{2\pi/(\ln(a/2\pi r_0) + 0.5275)}/a$  and  $k_c^2 = -\epsilon_h k_p^2 / f(\epsilon_m - \epsilon_h)$ . For each of three effective media, the value  $|k_c|$  is smaller than  $k_p$  within the range  $\lambda = 1.5\text{--}4.5\ \mu\text{m}$ . Therefore, one of the two TM-waves is quasi-TEM, and the other one, which corresponds to sign minus in (13), is the evanescent wave. For simplicity of writing, we report here the study in which we have neglected the evanescent eigenwave in semi-infinite effective media 1 and 3. The excitation of this TM-wave in media 1 and 3 by the quasi-TEM wave incident from medium 1 holds at both boundaries  $y=0$  and  $y=h$ . However, in media 1 and 3, this effect is very weak and has no impact to the transmittance. It is enough to take into account the evanescent solution only for medium 2. The expression for the magnetic field (which is in our case a one-component vector directed along  $z$ ) is as follows:

$$H(x, y, z) = H_0 e^{ik_x x + ik_z z} \begin{cases} e^{i\beta_1 y} + R e^{-i\beta_1 y} & y < 0 \\ g & 0 < y < h, \\ t e^{i\beta_3(y-h)} & y > h \end{cases} \quad (14)$$

in which  $g = A_1 e^{i\beta_2^{(1)} y} + A_2 e^{-i\beta_2^{(1)} y} + B_1 e^{i\beta_2^{(2)} y} + B_2 e^{-i\beta_2^{(2)} y}$ . Here,  $A_1$ ,  $A_2$ ,  $B_1$ , and  $B_2$  are the unknown amplitudes of the TM-polarized waves in layer 2,  $R$  and  $t$  are the reflection and transmission coefficients, respectively,  $\beta_1$  and  $\beta_3$  are the propagation factors of the quasi-TEM wave in hyperbolic media 1 and 3. Transverse components of the wave vector are preserved across boundaries and related to the spatial frequency  $q$  by the evident formula  $q = \sqrt{k_x^2 + k_z^2}$ . Boundary conditions (Maxwell's and additional ones) can be written as follows:<sup>64</sup>

$$[H_z] = 0, [E_x] = 0, \left[ \frac{1}{\epsilon^\perp} \frac{d^2 H_z}{dy^2} + k_0^2 H_z \right] = 0, \quad (15)$$

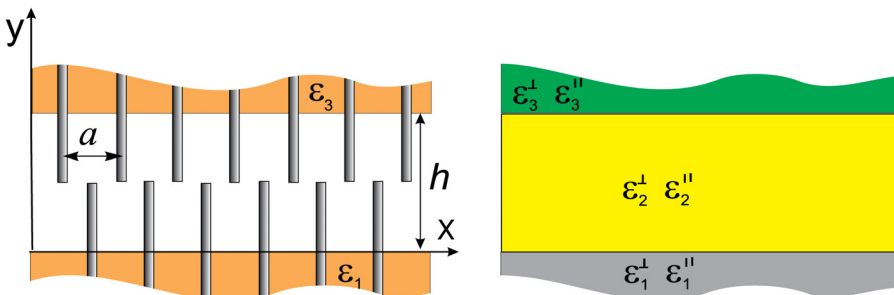


FIG. 11. Schematic view of the fourth structure under study, left hand figure, and its effective-medium model, right hand figure.

where the brackets [...] denote the jump discontinuities of given quantities at the interfaces  $y=0$  and  $y=h$ . Boundary conditions (15) at these interfaces combined with (14) result in the matrix equation:  $[M]\bar{X} = \bar{C}$ , where

$$\begin{aligned} \bar{X} &= [R, A_1, A_2, B_1, B_2, t]^T, \\ \bar{C} &= [1, Z_a, \frac{[\beta_1]^2}{Z_a}, 0, 0, 0]^T, \\ [M] &= [[M_1], [M_2]], \end{aligned} \quad (16)$$

and

$$[M_1] = \begin{bmatrix} -1 & 1 & 1 \\ Z_a & Z_1 & -Z_1 \\ \frac{[\beta_1]^2}{\epsilon_a} & \frac{[\beta_2^{(1)}]^2}{\epsilon_t} & \frac{[\beta_2^{(1)}]^2}{\epsilon_t} \\ 0 & \frac{[\beta_2^{(1)}]^2}{\epsilon_t} e^{i\beta_2^{(1)}h} & \frac{[\beta_2^{(1)}]^2}{\epsilon_t} e^{-i\beta_2^{(1)}h} \\ 0 & Z_1 e^{i\beta_2^{(1)}h} & -Z_1 e^{-i\beta_2^{(1)}h} \\ 0 & Z_1 e^{i\beta_2^{(1)}h} & -Z_1 e^{-i\beta_2^{(1)}h} \end{bmatrix}, \quad (17)$$

$$[M_2] = \begin{bmatrix} 1 & 1 & 0 \\ Z_2 & -Z_2 & 0 \\ \frac{[\beta_2^{(2)}]^2}{\epsilon_t} & \frac{[\beta_2^{(2)}]^2}{\epsilon_t} & 0 \\ \frac{[\beta_2^{(2)}]^2}{\epsilon_t} e^{i\beta_2^{(2)}h} & \frac{[\beta_2^{(2)}]^2}{\epsilon_t} e^{-i\beta_2^{(2)}h} & -\frac{[\beta_3]^2}{\epsilon_b} \\ e^{i\beta_2^{(2)}h} & e^{-i\beta_2^{(2)}h} & -1 \\ Z_2 e^{i\beta_2^{(2)}h} & -Z_2 e^{-i\beta_2^{(2)}h} & -Z_b \end{bmatrix}.$$

In the above formulas, we use following notations:  $\epsilon_t = \epsilon_2^\perp$ ,  $\epsilon_a = \epsilon_1^\perp$ ,  $\epsilon_b = \epsilon_3^\perp$ ,  $Z_{1,2} = \sqrt{\mu_0/\epsilon_0} \beta_2^{(1,2)}/\epsilon_t$ ,  $Z_{a,b} = \sqrt{\mu_0/\epsilon_0} \beta_{1,3}/\epsilon_{a,b}$ . Solving numerically the matrix equation, we find the amplitude of the transmission coefficient  $t$  and the normalized power transmittance  $N$ . This is the non-local variant of EMM. The simplified variant has been described above. Optical constants of SiC were taken from Ref. 71. Nanowires have the thickness  $2r_0=40$  nm and their array has the period  $a=100$  nm.

## B. Results

The results for  $N(\omega, q)$  versus  $qa$  (spatial frequency multiplied by array period) at several frequencies are shown in Fig. 12. Fabry-Perot resonances due to the imperfect matching are explicitly visible in the transmittance over the broad spatial spectrum in which RHT holds in the present case. The spatial dispersion gives a significant decrease of  $N$  compared to the predictions of the simplified EMM (without any shift versus  $qa$  or other qualitative changes in the curves). This impact of spatial dispersion is so strong in the present case because all three effective media are hyperbolic. In the simplified version of EMM, there is practically no reflection at the interfaces, and all the heat is transferred. In fact, when

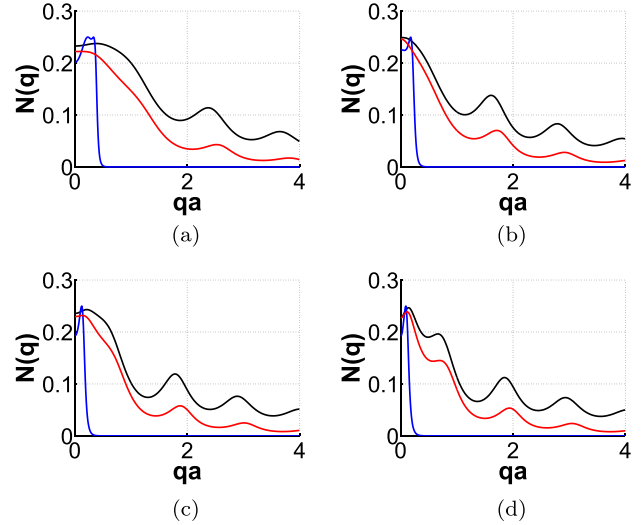


FIG. 12.  $N$  versus  $qa$  (spatial frequency multiplied by array period), calculated for the gold nanowires at the frequencies: (a)  $f=200$  THz ( $\lambda=1.5 \mu\text{m}$ ), (b)  $f=120$  THz ( $\lambda=2.5 \mu\text{m}$ ), (c)  $f=85.71$  THz ( $\lambda=3.5 \mu\text{m}$ ), and (d)  $f=66.66$  THz ( $\lambda=4.5 \mu\text{m}$ ). Blue curves correspond to the absence of nanowires in the gap (nanowires are kept in media 1 and 3), black curves correspond to the simplified variant of EMM, and red curves correspond to the non-local model. Radius of wires  $r_0=20$  nm, period of the WM lattice  $a=100$  nm, thickness of the gap  $h=1 \mu\text{m}$ .

all three media are WMMs and the matching is good, both modes (quasi-TEM and evanescent TM ones) are efficiently excited in medium 2. This implies a noticeable reflection especially for high spatial frequencies  $q \sim \pi/a$ . This reflection is so due to low optical losses in gold. Notice that in our previous (frequency selective) structures the similar effect obviously holds in the frequency regions where the impedance matching is good and the power transmittance is maximal. At these frequencies, the simplified EMM gives optimistic predictions.

If we replace gold by a more lossy metal, such as tungsten, the excitation of the evanescent TM-wave weakens and the simplified model becomes more adequate. Fig. 13 is an analogue of Fig. 12, where Au nanowires are replaced by W ones. In the present structure where the impact of spatial dispersion is maximal, the excitation of the evanescent TM-wave still remains noticeable, and the spatial dispersion still reduces the transmittance. However, this reduction is not so significant as for gold—it nearly equals to 25–30%. Also, Fabry-Perot resonances disappear—the impact of internal reflections is suppressed by the wave decay. Anyway, even for tungsten nanowires RHT still keeps strongly super-Planckian.

In Fig. 14, we present the results for RHT function  $M(\omega)$  calculated for several cases. All solid curves correspond to Au nanowires, all dashed curves correspond to W nanowires. Blue curves correspond to the case when nanowires are absent in the gap, however, they are present in both media 1 and 3. These hyperbolic metamaterials are identical and mimic the black body (in what concerns their far-field radiation). Therefore, RHT in the case of the vacuum gap turns out to be practically equal to that between two black bodies. Solid and dashed blue curves almost coincide. It means that the impact of gold and tungsten nanowires is

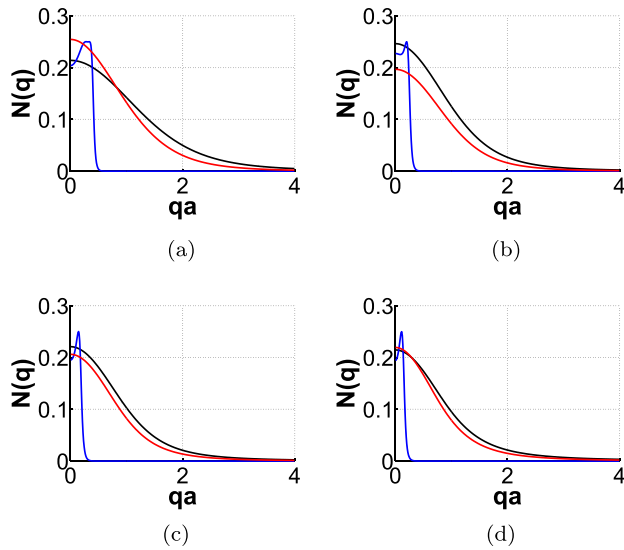


FIG. 13.  $N$  versus  $qa$ , calculated for the tungsten nanowires at the frequencies: (a)  $f=200$  THz ( $\lambda=1.5$   $\mu\text{m}$ ), (b)  $f=120$  THz ( $\lambda=2.5$   $\mu\text{m}$ ), (c)  $f=85.71$  THz ( $\lambda=3.5$   $\mu\text{m}$ ), and (d)  $f=66.66$  THz ( $\lambda=4.5$   $\mu\text{m}$ ). Blue curves correspond to the absence of nanowires in the gap, black curves correspond to the simplified variant of EMM, and red curves correspond to the non-local model. Geometric parameters are same as above.

nearly equivalent—in both cases, media 1 and 3 are effective black bodies. Black solid curve corresponds to Au nanowires in the gap and the use of the simplified EMM, which predicts the largest gain compared to RHT between black bodies. Depending on the frequency, this gain changes from 100 to 600 in the range of 60–200 THz. Red solid curve corresponds to Au nanowires in the gap and the non-local EMM. Its result for RHT is nearly 5 times smaller than that predicted by the simplified model. However, being averaged over the range of 60–200 THz it still keeps nearly 100 times larger than RHT between black bodies. For W nanowires (black dashed and red dashed curves), the spatial dispersion decreases RHT nearly by 30% compared to the simplified model. Again, in both variants of EMM model RHT keeps much higher than that between black bodies. The simplified version gives the averaged gain (of RHT compared to black bodies) nearly equal to 75, the non-local version—nearly 50.

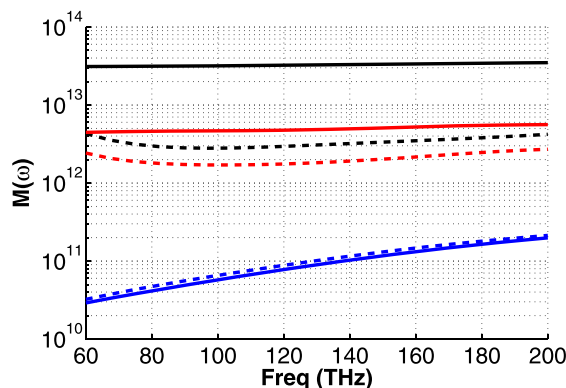


FIG. 14. Radiative heat transfer function  $M$  calculated for gold (solid curves) and tungsten (dashed curves) nanowires in the logarithmic scale. Blue curves correspond to the absence of nanowires in the gap. Black curves determine the case that we do not consider additional TM-wave, and red curves represent the case that we take into account additional TM-wave.

## VI. CONCLUSION

In this paper, we have presented a comprehensive study of the applicability of effective media models for calculating the radiative heat transfer through metamaterials formed by arrays of metal nanowires. For this purpose, we compared the predictions of effective models with results of full-wave simulations for geometrical set-ups typical for thermophotovoltaic devices. For the case of nanowires within the micron-thick gap between emitter and absorber, we found that a simple local formulation of the effective medium model leads to a reasonable qualitative agreement of the predicted total heat transfer rate and of the significant frequency range with the results of full-wave simulations. These results show that the effective medium model is a powerful tool for designing, analyzing, and optimizing this class of devices. Our results for devices in which both emitter and absorber made of nanowired media show that in this case the situation becomes more complicated because the evanescent mode of the wired medium comes into play. The contribution of this mode requires at least the usage of a non-local effective medium model.

<sup>1</sup>D. R. Smith and D. Schurig, *Phys. Rev. Lett.* **90**, 077405 (2003).

<sup>2</sup>J. Kim, V. P. Drachev, Z. Jacob, G. V. Naik, A. Boltasseva, E. E. Narimanov, and V. M. Shalaev, *Opt. Express* **20**, 8100–8116 (2012).

<sup>3</sup>A. N. Poddubny, P. A. Belov, and Yu. S. Kivshar, *Phys. Rev. A* **84**, 023807 (2011).

<sup>4</sup>M. A. Noginov, Yu. A. Barnakov, T. Zhu, T. Tumkur, H. Li, and E. E. Narimanov, *Appl. Phys. Lett.* **94**, 151105 (2009).

<sup>5</sup>A. Poddubny, I. Iorsh, P. Belov, and Yu. S. Kivshar, *Nature Photon.* **7**, 948–957 (2013).

<sup>6</sup>R. K. Fisher and R. W. Gould, *Phys. Rev. Lett.* **22**, 1093–1095 (1969).

<sup>7</sup>S.-A. Biehs, M. Tschikin, and P. Ben-Abdallah, *Phys. Rev. Lett.* **109**, 104301 (2012).

<sup>8</sup>B. Liu and S. Shen, *Phys. Rev. B* **87**, 115403 (2013).

<sup>9</sup>S.-A. Biehs, M. Tschikin, R. Messina, and P. Ben-Abdallah, *Appl. Phys. Lett.* **102**, 131106 (2013).

<sup>10</sup>I. S. Nefedov and C. R. Simovski, *Phys. Rev. B* **84**, 195459 (2011).

<sup>11</sup>M. Tschikin, P. Ben-Abdallah, and S.-A. Biehs, *Phys. Lett. A* **376**, 3462 (2012).

<sup>12</sup>Y. Guo and Z. Jacob, *Optics Express* **21**, 15014–15019 (2013).

<sup>13</sup>S. Molesky, C. J. Dewalt, and Z. Jacob, *Optics Express* **21**, A96–A110 (2013).

<sup>14</sup>Y. Guo, C. L. Cortes, S. Molesky, and Z. Jacob, *Appl. Phys. Lett.* **101**, 131106 (2012).

<sup>15</sup>I. S. Nefedov, L. A. Melnikov, and E. I. Nefedov, *Proc. SPIE* **8771**, 87710K (2013).

<sup>16</sup>C. Simovski, S. Maslovski, I. Nefedov, and S. Tretyakov, *Opt. Express* **21**, 14988–15013 (2013).

<sup>17</sup>M. G. Mauk, *Survey of Thermophotovoltaic (TPV) Devices* (Springer, Berlin–Heidelberg, 2007).

<sup>18</sup>T. Bauer, *Thermophotovoltaics: Basic Principles and Critical Aspects of System Design* (Springer, Berlin–Heidelberg, 2011).

<sup>19</sup>F. Demichelis, E. Minettmezzetti, M. Agnello, and E. Tresso, *J. Appl. Phys.* **53**, 9098–9104 (1982).

<sup>20</sup>E. Rephaeli and S. Fan, *Optics Express* **17**(17), 15145–15159 (2009).

<sup>21</sup>P. Bermel, M. Ghebrebrhan, W. Chan, Y.-X. Yeng, M. Araghchini, R. Hamam, C. H. Marton, K. F. Jensen, M. Soljacic, J. D. Joannopoulos, S. G. Johnson, and I. Celanovic, *Opt. Express* **18**, A314–A334 (2010).

<sup>22</sup>C. Wu, B. Neuner III, J. John, A. Milder, B. Zollars, S. Savoy, and G. Shvets, *J. Opt.* **14**, 024005 (2012).

<sup>23</sup>D. Chester, P. Bermel, J. D. Joannopoulos, M. Soljacic, and I. Celanovic, *Opt. Express* **19**(S3), A245–A257 (2011).

<sup>24</sup>M. De Zoysa, T. Asano, K. Mochizuki, A. Oskooi, T. Inoue, and S. Noda, *Nature Photon.* **6**, 535–539 (2012).

<sup>25</sup>A. Lenert, D. M. Bierman, Y. Nam, W. R. Chan, I. Celanovic, M. Soljacic, and E. N. Wang, *Nature Nanotechnol.* **9**, 126–130 (2014).

- <sup>26</sup>S. M. Rytov, *Theory of Electric Fluctuations and Thermal Radiation* (Electronics Research Directorate, Air Force Cambridge Research Center, Air Research and Development Command, U.S. Air Force, 1959).
- <sup>27</sup>D. Polder and M. van Hove, *Phys. Rev. B* **4**, 3303–3314 (1971).
- <sup>28</sup>H. B. Callen and T. A. Welton, *Phys. Rev.* **83**, 34–49 (1951).
- <sup>29</sup>R. Landauer, *IBM J. Res. Dev.* **5**, 183–191 (1961).
- <sup>30</sup>C. M. Hargreaves, *Phys. Lett. A* **30**, 491–492 (1969).
- <sup>31</sup>J. B. Pendry, *J. Phys.: Condens. Matter* **11**, 6621–6633 (1999).
- <sup>32</sup>J.-P. Mulet, K. Joulain, R. Carminati, and J.-J. Greffet, *Appl. Phys. Lett.* **78**, 2931 (2001).
- <sup>33</sup>R. Hillenbrand, T. Taubner, and F. Keilmann, *Nature* **418**, 159–162 (2002).
- <sup>34</sup>A. I. Volokitin and B. N. J. Persson, *Phys. Rev. B* **69**, 045417 (2004).
- <sup>35</sup>K. Joulain, J.-P. Mulet, F. Marquier, R. Carminati, and J.-J. Greffet, *Surf. Sci. Rep.* **57**, 59–112 (2005).
- <sup>36</sup>M. Laroche, R. Carminati, and J.-J. Greffet, *J. Appl. Phys.* **100**, 063704 (2006).
- <sup>37</sup>K. Joulain, *J. Quant. Spectrosc. Radiat. Transfer* **109**, 294–304 (2008).
- <sup>38</sup>J. B. Xu, K. Luger, R. Moller, K. Dransfeld, and I. H. Wilson, *J. Appl. Phys.* **76**, 7209 (1994).
- <sup>39</sup>E. Rousseau, A. Siria, G. Jourdan, S. Volz, F. Comin, J. Chevrier, and Jean-Jacques Greffet, *Nature Photon.* **3**, 514–519 (2009).
- <sup>40</sup>R. S. Ottens, V. Quetschke, S. Wise, A. A. Alemi, R. Lundock, G. Mueller, D. H. Reitze, D. B. Tanner, and B. F. Whiting, *Phys. Rev. Lett.* **107**, 014301 (2011).
- <sup>41</sup>S. Basu, Z. M. Zhang, and C. J. Fu, *Int. J. Energy Res.* **33**, 1203–1232 (2009).
- <sup>42</sup>C. Fu and Z. M. Zhang, *Front. Energy Power Eng. China* **3**, 11–26 (2009).
- <sup>43</sup>A. Kittel, W. Muller-Hirsch, J. Parisi, S.-A. Biehs, D. Reddig, and M. Holthaus, *Phys. Rev. Lett.* **95**, 224301 (2005).
- <sup>44</sup>T. Kralik, P. Hanzelka, V. Musilova, A. Srnka, and M. Zobac, *Rev. Sci. Instrum.* **82**, 055106 (2011).
- <sup>45</sup>P. J. van Zwol, S. Thiele, C. Berger, W. A. de Heer, and J. Chevrier, *Phys. Rev. Lett.* **109**, 264301 (2012).
- <sup>46</sup>B. V. Budaev and D. B. Bogy, *Ann. Phys. (Berlin)* **523**(10), 791–804 (2011).
- <sup>47</sup>S. Basu, Y.-B. Chen, and Z. M. Zhang, *Int. J. Energy Res.* **31**, 689–716 (2007).
- <sup>48</sup>A. Kittel, U. F. Wischnath, J. Welker, O. Huth, F. Ruting, and S.-A. Biehs, *Appl. Phys. Lett.* **93**, 193109 (2008).
- <sup>49</sup>M. I. Flik, B. I. Choi, and K. E. Goodson, *J. Heat Transfer* **114**, 666–674 (1992).
- <sup>50</sup>M. D. Whale and E. G. Cravalho, *IEEE Trans. Energy Convers.* **17**, 130–137 (2002).
- <sup>51</sup>B. Wernsman, R. R. Siergiej, S. D. Link, R. G. Mahorter, M. N. Palmisiano, R. J. Wehrer, R. W. Schultz, G. P. Schmuck, R. L. Messham, S. Murray, C. S. Murray, F. Newman, D. Taylor, D. M. DePoy, and T. Rahmlow, *IEEE Trans. Electron. Dev.* **51**, 512–515 (2004).
- <sup>52</sup>R. DiMatteo, P. Greiff, D. Seltzer, D. Meulenberg, E. Brown, E. Carlen, K. Kaiser, S. Finberg, H. Nguyen, J. Azarkevich, P. Baldasaro, J. Beausang, L. Danielson, M. Dashiell, D. DePoy, H. Ehsani, W. Topper, K. Rahner, and R. Siergiej, in *Proc. 6th Conference on Thermophotovoltaic Generation of Electricity, TPV6, Freiburg, Germany* (2004), pp. 42–51.
- <sup>53</sup>T. Bauer, I. Forbes, R. Penlington, and N. Pearsall, *Sol. Energy Mater. Sol. Cells* **88**, 257–268 (2005).
- <sup>54</sup>J. Baxter, Z. Bian, G. Chen, D. Danielson, M. S. Dresselhaus, A. G. Fedorov, T. S. Fisher, C. W. Jones, E. Maginn, U. Kortshagen, A. Manthiram, A. Nozik, D. R. Rolison, T. Sands, L. Shi, D. Sholl, and Y. Wu, *Energy Environ. Sci.* **2**, 559–588 (2009).
- <sup>55</sup>R. S. DiMatteo, M. S. Weinberg, and G. A. Kirkos, US Patent 2001/6232546 B1.
- <sup>56</sup>D. M. Matson and R. Venkatesh, US Patent 2006/0289310 A1.
- <sup>57</sup>P. Greiff, R. DiMatteo, E. Brown, and C. Leitz, US Patent 2010/0319749 A1.
- <sup>58</sup>A. V. Kabashin, P. Evans, S. Pastkovsky, W. Hendren, G. A. Wurtz, R. Atkinson, R. Pollard, V. A. Podolskiy, and A. V. Zayats, *Nature Mater.* **8**, 867–871 (2009).
- <sup>59</sup>S. I. Maslovski, C. R. Simovski, and S. A. Tretyakov, *Phys. Rev. B* **87**, 155124 (2013).
- <sup>60</sup>M. Tschikin, S.-A. Biehs, R. Messina, and P. Ben-Abdallah, *J. Opt.* **15**, 105101 (2013).
- <sup>61</sup>M. Silveirinha, *Phys. Rev. E* **73**, 046612 (2006).
- <sup>62</sup>M. G. Silveirinha, P. A. Belov, and C. R. Simovski, *Phys. Rev. B* **75**, 035108 (2007).
- <sup>63</sup>S. Maslovski and M. Silveirinha, *Phys. Rev. B* **80**, 245101 (2009).
- <sup>64</sup>M. G. Silveirinha, *IEEE Trans. Antennas Propagat.* **54**, 1766–1773 (2006).
- <sup>65</sup>A. V. Chebykin, A. A. Orlov, A. V. Vozianova, S. I. Maslovski, Yu. S. Kivshar, and P. A. Belov, *Phys. Rev. B* **84**, 115438 (2011).
- <sup>66</sup>A. V. Chebykin, A. A. Orlov, C. R. Simovski, Yu. S. Kivshar, and P. A. Belov, *Phys. Rev. B* **86**, 115420 (2012).
- <sup>67</sup>C. R. Simovski, P. A. Belov, A. V. Atraschenko, and Yu. S. Kivshar, *Adv. Mater.* **24**, 4229–4248 (2012).
- <sup>68</sup>J. Brown and W. Jackson, *Proc. IEE – Part B: Radio and Electr.* **102**, 11–16 (1955).
- <sup>69</sup>M. A. Ordal, Robert J. Bell, R. W. Alexander, Jr., L. L. Long, and M. R. Querry, *Appl. Opt.* **24**(24), 4493–4502 (1985).
- <sup>70</sup>P. Yeh, A. Yariv, and C.-S. Hong, *J. Opt. Soc. Am.* **67**(4), 423–438 (1977).
- <sup>71</sup>E. D. Palik, *Handbook of Optical Constants of Solids* (Academic Press, San Diego, 1998).